Science of the Total Environment 627 (2018) 523–533

Contents lists available at ScienceDirect

Science of the Total Environment

journal homepage: www.elsevier.com/locate/scitotenv

Modeling crop residue burning experiments to evaluate smoke emissions and plume transport

Luxi Zhou [a,b,*], Kirk R. Baker [a], Sergey L. Napelenok [a], George Pouliot [a], Robert Elleman [c], Susan M. O'Neill [d], Shawn P. Urbanski [e], David C. Wong [a]

[a] U.S. Environmental Protection Agency, Research Triangle Park, NC 27711, United States
[b] National Academies of Science, Engineering and Medicine, Washington, DC 20001, United States
[c] U.S. Environmental Protection Agency, Region 10, Seattle, WA 98101, United States
[d] U.S. Forest Service, Pacific Northwest Research Station, Seattle, WA 98103, United States
[e] U.S. Forest Service, Fire Sciences Laboratory, Missoula, MT 59808, United States

HIGHLIGHTS

- Detailed evaluation of fuel loading and emission factors of $PM_{2.5}$ and CO for bluegrass and winter wheat fuel types.
- 30% to 200% underestimation in buoyancy heat flux with default field information underestimate plume height up to 80.
- Improved plume structure modeling for crop residual burning with field measurements based buoyancy heat flux estimation.

GRAPHICAL ABSTRACT

ARTICLE INFO

Article history:
Received 9 November 2017
Received in revised form 24 January 2018
Accepted 24 January 2018
Available online xxxx

Editor: Jianmin Chen

Keywords:
Air quality modeling
Biomass burning
Emissions
Smoke plume
CMAQ

ABSTRACT

Crop residue burning is a common land management practice that results in emissions of a variety of pollutants with negative health impacts. Modeling systems are used to estimate air quality impacts of crop residue burning to support retrospective regulatory assessments and also for forecasting purposes. Ground and airborne measurements from a recent field experiment in the Pacific Northwest focused on cropland residue burning was used to evaluate model performance in capturing surface and aloft impacts from the burning events. The Community Multiscale Air Quality (CMAQ) model was used to simulate multiple crop residue burns with 2 km grid spacing using field-specific information and also more general assumptions traditionally used to support National Emission Inventory based assessments. Field study specific information, which includes area burned, fuel consumption, and combustion completeness, resulted in increased biomass consumption by 123 tons (60% increase) on average compared to consumption estimated with default methods in the National Emission Inventory (NEI) process. Buoyancy heat flux, a key parameter for model predicted fire plume rise, estimated from fuel loading obtained from field measurements can be 30% to 200% more than when estimated using default field information. The increased buoyancy heat flux resulted in higher plume rise by 30% to 80%. This evaluation indicates that the regulatory air quality modeling system can replicate intensity and transport (horizontal and vertical) features for crop residue burning in this region when region-specific information is used to inform emissions and plume rise calculations. Further, previous vertical emissions allocation treatment of putting all cropland

* Corresponding author at: U.S. Environmental Protection Agency, Research Triangle Park, NC 27711, United States.
E-mail address: zhou.luxi@epa.gov (L. Zhou).

https://doi.org/10.1016/j.scitotenv.2018.01.237

residue burning in the surface layer does not compare well with measured plume structure and these types of burns should be modeled more similarly to prescribed fires such that plume rise is based on an estimate of buoyancy.

1. Introduction

Crop residue burning is commonly used in agricultural land management to dispose of crop residue and provide other benefits such as pest control and ash generation for fertilization (McCarty, 2011). However, pollution from open biomass burning has been linked to negative human health impacts (Liu et al., 2016; Reid et al., 2016; Liu et al., 2015; Rappold et al., 2011). In addition, particles emitted from fires have direct radiative effects and contribute cloud condensation nuclei which have indirect effects (Yu et al., 2016; Forster et al., 2007). Nationally, approximately 1.2 million ha of croplands are burned annually on average, which is equivalent to 43% of the annual average area of wild fires in the U.S. (McCarty et al., 2009). The Pacific Northwest is a region of major agricultural burning, with cropland burning of nearly 200,000 ha per year (McCarty et al., 2009). Photochemical transport models have been used to support scientific and regulatory assessments that quantify the impact of wildland fires and cropland burning on O_3 and $PM_{2.5}$ (Baker et al., 2016; Fann et al., 2013; Jain et al., 2007). In those studies, differences between model predictions and ambient measurements were partially explained by uncertainty in meteorological input fields and fire emissions (Garcia-Menendez et al., 2013; Seaman, 2000; USDA Forest Service, 1998; Urbanski et al., 2011). Numerous laboratory experiments have been conducted to quantify biomass burning emission factors, but the accuracy of applying these emission factors for open biomass burning is still uncertain (Holder et al., 2017; Aurell and Gullett, 2013; Aurell et al., 2015; Dhammapala et al., 2006). In addition to the magnitude of emission rates, the spatial and temporal allocation of emissions is critical to sufficiently describing the fire smoke impacts (Larkin et al., 2012; Garcia-Menendez et al., 2014). In particular, plume rise height is important in terms of how fire emissions are transported and chemically transformed which impacts total residence time in the atmosphere and ambient pollutant levels (Paugam et al., 2016).

The relative composition and magnitude of emissions from fires varies due to meteorology, fuel type, combustion efficiency, and fire size (Urbanski et al., 2011; Wiedinmyer and Hurteau, 2010). Field data from specific and well characterized fires is critically important to improve emission estimation approaches for fires and plume transport in photochemical transport models. Field measurements have been made downwind of cropland burning, but rarely include information about the type of fuel burned, amount of fuel burned, and the area burned (Liu et al., 2016). In other studies, fuels are well characterized but lack downwind plume characterization (Washington State University, 2004; U.S. EPA, 2003). A field study in eastern Washington and northern Idaho in August 2013 consisted of multiple burns of well characterized fuels with nearby surface and aerial measurements including trace species concentrations, plume rise height and boundary layer structure (Holder et al., 2017). The ground-based, airborne and remote sensing data from this campaign provides a unique opportunity to assess how well a regulatory modeling system quantifies the air quality impacts of cropland residue fires by characterizing emissions and subsequent vertical plume transport.

Here, surface and aerial measurements taken during the August 2013 field study in eastern Washington and northern Idaho (Holder et al., 2017) are used to evaluate the cropland burning emission estimation approach (Pouliot et al., 2017) used to support regulatory air quality modeling. Field specific data were used in place of typical assumptions for regulatory modeling to evaluate how well plume rise and near-fire transport are characterized for cropland burning in the Pacific Northwest using the Community Multiscale Air Quality (CMAQ) model. The sensitivity of modeled plume rise is explored using CMAQ by varying input assumptions and using actual field data where possible. Analysis is focused on ground-based ($PM_{2.5}$ and CO) and downwind (CO) field measurements since information is available at the emission factor scale (ground level in-plume) and grid scale (aircraft downwind in-plume). Improved emissions and model approaches for cropland plume transport can help improve regulatory modeling (e.g., State Implementation Plans), forecasting systems (e.g., AIRPACT), and smoke management programs.

2. Materials and methods

2.1. Observations

All observation data used in this study were obtained from the crop residue burning field experiment in the Pacific Northwest (Holder et al., 2017). Fig. 1 shows the location of the Nez Perce and Walla Walla instrumented burns along with nearby wildland (wild and prescribed) fires. The Nez Perce burns were at higher elevation and closer to more complex terrain compared to the Walla Walla burns. Specific fields burned and nearby surface and aerostat measurements are shown for both Nez Perce in Fig. 2 and Walla Walla in Fig. 3. Four fields of Kentucky bluegrass and one field of winter wheat were burned in Nez Perce, Idaho during 19–20 August 2013 and three fields of winter wheat were burned in Walla Walla, Washington during 24–25 August 2013. Fields at Nez Perce were squares and similar in area. Burns happened in both the late morning and afternoon on August 19 and 20 at Nez Perce. The fields at Walla Walla were irregularly shaped and follow natural terrain features with roads used as fire breaks. The location, duration, field size, fuel type, and fuel load for each burn are listed in Table 1 with additional details in Table S1. Burn 7 was not sampled by the aircraft and not included as part of this analysis.

Aerial (aerostat and airplane) sampling was employed to measure $PM_{2.5}$ and gases including CO and carbon dioxide (CO_2) during the burning. Ground-based measurements of $PM_{2.5}$ were provided by multiple Environmental Beta Attenuation Monitors (EBAMs, Met One Inc., Grants Pass, OR) arrayed downwind of each burn measuring at 10-min and hourly average intervals. Remote sensing instruments were deployed to detect boundary layer height (ceilometer) and smoke plume top (lidar) (Kovalev et al., 2015). The location of ground monitors, aerostat, and remote sensing instruments are indicated in Figs. 2 and 3 and colored to match the field burned. The Modified Combustion Efficiency (MCE) was calculated as $\Delta CO_2 / (\Delta CO_2 + \Delta CO)$, where ΔCO_2 and ΔCO are the mixing ratio enhancements of these gases above background. MCE was used as a metric to subjectively describe fire as flaming (MCE > 0.95) or smoldering (MCE < 0.90). A detailed description of the field experiment including surface, aerostat, and aircraft observation data are provided in Holder et al. (2017).

2.2. Model configuration and inputs

The CMAQ model version 5.2 (Byun and Schere, 2006; Foley et al., 2010) was applied from August 18 to 28, 2013 to match the period of instrumented crop residue fires set in southeast Washington state and northern Idaho. The model simulated emissions, transport, and physical/chemical transformation of primary and secondary pollutants (e.g. O_3, $PM_{2.5}$) from all sources. Anthropogenic emissions (e.g. point, area, and mobile sources) were based on the 2011 version 2 National

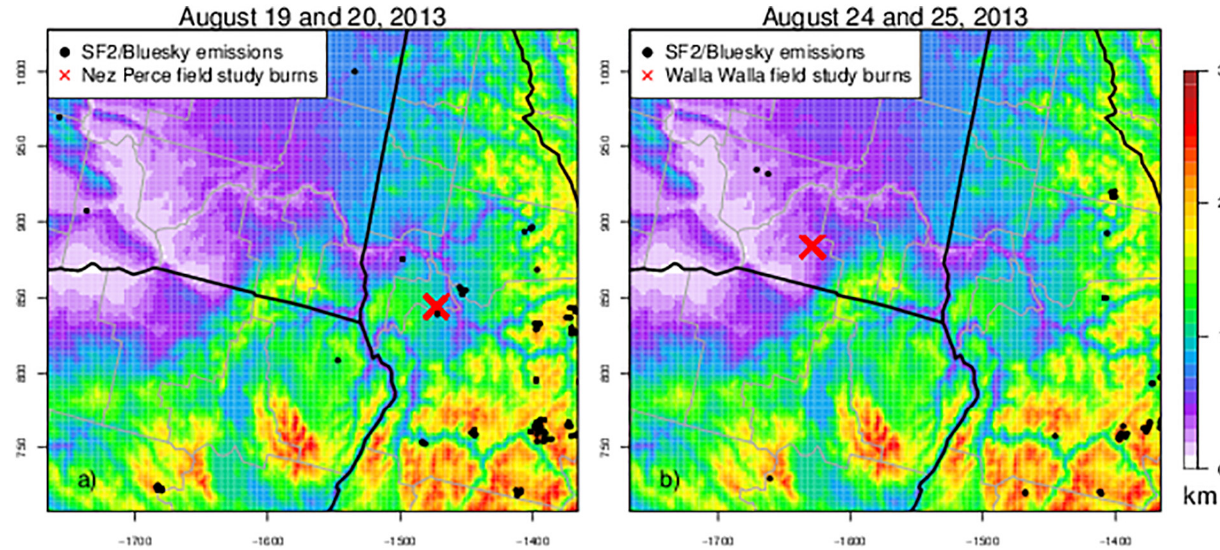

Fig. 1. Model domain with field study location and nearby wildland fires (dots) are shown for the burns at Nez Perce (a) and Walla Walla (b). Color shading represents terrain height where warm colors represent higher terrain elevations above ground level. (For interpretation of the references to color in this figure legend, the reader is referred to the web version of this article.)

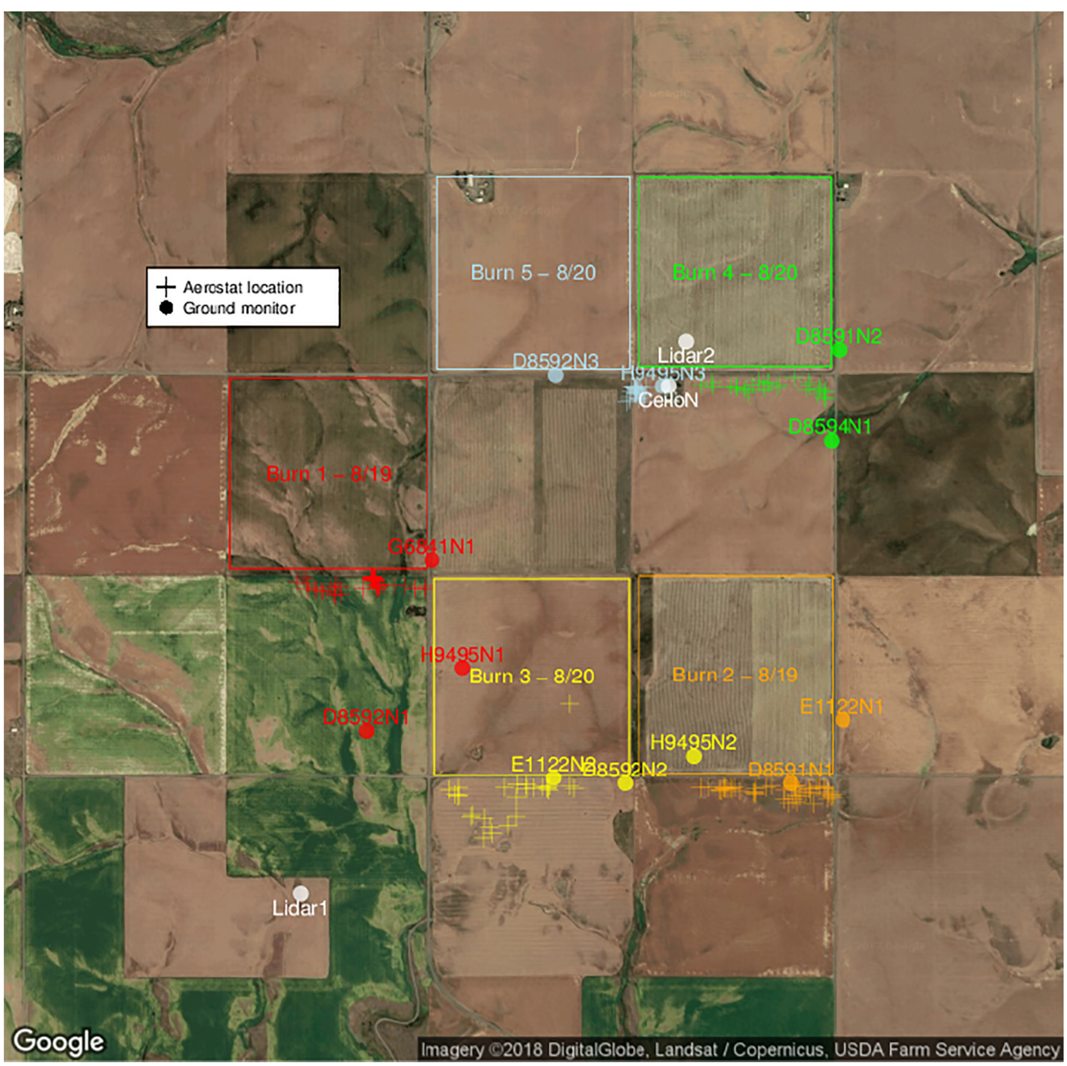

Fig. 2. Burn units 1 through 5 shown along with the location of ground-based and aerostat measurements at Nez Perce.

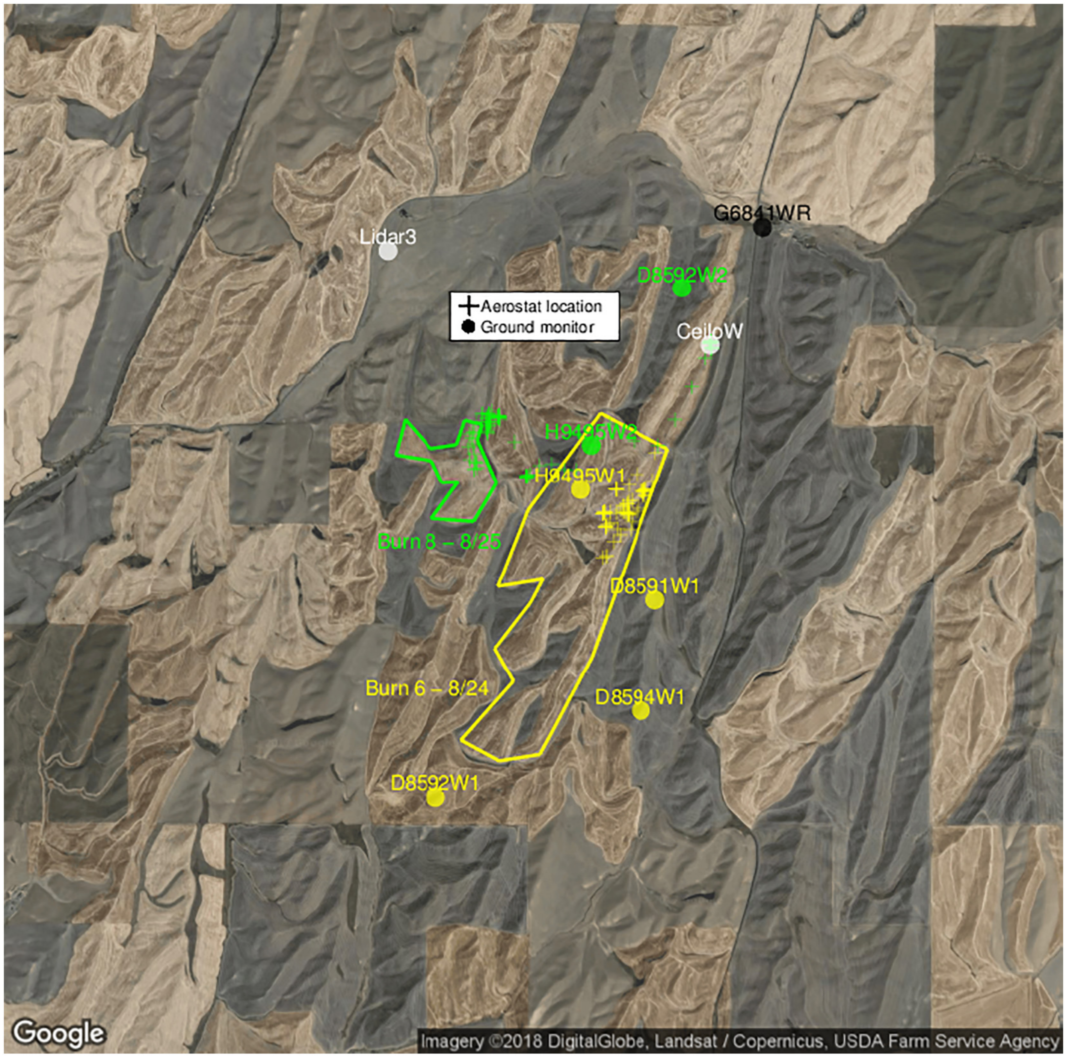

Fig. 3. Burn units 6 and 8 shown along with the location of ground-based and aerostat measurements at Walla Walla.

Emission Inventory (NEI) (U.S. EPA, 2016). Point source emissions were based on 2013 Continuous Emissions Monitoring information where available. Biogenic emissions were based on the Biogenic Emissions Inventory System (BEIS) version 3.6.1 (Bash et al., 2016). Wild and prescribed fires were based on 2013 day-specific location and timing information from satellite products and emissions estimates using the

Table 1
Fuel information (B = bluegrass, W = wheat) and emission factors (g pollutant/kg biomass consumed) used for developing CMAQ emission inputs for the simulation based on field study information (top section) and Pouliot et al., 2017 approach (bottom section). The MCE presented here is based on emission factors for CO and CO_2 (which are not shown).

Burn No.	Fuel type	Size (acres)	Fuel load (tons/acre)	Combustion completeness (%)	Biomass consumed (tons)	Approximate duration (h)	MCE	Emission factor		Total emissions (tons)	
								CO	$PM_{2.5}$	CO	$PM_{2.5}$
Field study based emissions and field information											
1	B	163	1.16	0.9	170	1	0.95	49.4	14.6	8.4	2.5
2	B	163	1.61	0.9	236	1	0.93	68.1	12.4	16.1	2.9
3	W	163	1.65	0.9	242	1	0.95	49.9	9.3	12.1	2.3
4	B	163	2.87	0.9	421	1	0.93	74.2	19	31.2	8.0
5	B	163	1.82	0.9	267	2	0.94	64.7	8.5	17.8	2.4
6	W	237	3.07	0.9	655	2	0.97	34.1	12.6	22.4	8.2
8	W	67	3.39	0.9	204	1	0.97	27	12.2	5.5	2.5
Pouliot et al., 2017 based emissions and assumptions about field information											
1	B	120	1.9	0.85	194	1	0.95	91.1	11.6	17.6	2.3
2	B	120	1.9	0.85	194	1	0.95	91.1	11.6	17.6	2.3
3	W	120	1.9	0.85	194	1	0.97	55.1	4.0	10.7	0.8
4	B	120	1.9	0.85	194	1	0.95	91.1	11.6	17.6	2.3
5	B	120	1.9	0.85	194	2	0.95	91.1	11.6	17.6	2.3
6	W	120	1.9	0.85	194	2	0.97	55.1	4.0	10.7	0.8
8	W	120	1.9	0.85	194	1	0.97	91.1	4.0	10.7	0.8

Smartfire2/BlueSky framework (Baker et al., 2016; Larkin et al., 2009). The approach for cropland emissions estimation is presented in Section 2.3.

The Weather Research and Forecasting (WRF) model (NCAR, 2008) was applied to generate meteorological inputs for CMAQ. WRF and CMAQ were both applied with the same lambert conic conformal projection for a domain covering eastern Washington and northern Idaho using 200 × 160 2 km sized square grid cells (shown in Fig. 1). A total of 35 layers were used to resolve the troposphere up to 50 mb with thinner layers near the surface to best resolve diurnal variation in the surface mixing layer. Initial conditions and boundary chemical inflow were extracted from an annual 2013 CMAQ simulation that covered the entire continental United States using 12 km sized grid cells (Henderson et al., 2014). CMAQ was applied with Carbon Bond based gas phase chemistry (Sarwar et al., 2011), ISORROPIA II inorganic thermodynamics (Fountoukis and Nenes II, 2007), aqueous phase chemistry (Sarwar et al., 2013), and 2-product semi-volatile organic aerosol partitioning scheme using laboratory-based secondary organic aerosol (SOA) yields from gas phase precursors including isoprene, monoterpenes, sesquiterpenes, toluene, xylene, and benzene (Carlton et al., 2010).

2.3. Cropland fire emissions treatment

Fire smoke emission rates were prepared to demonstrate the differences in simulated pollutant concentrations based on two different approaches for estimating emissions. One approach is based on available field study information and the other on information provided in Pouliot et al., 2017, which is the approach traditionally used to support regulatory assessments (Table 1 and Table S2). Table 1 presents field specific information used for preparing fire smoke emissions using each approach. The Sparse Matrix Operations Kernel Emissions (SMOKE) processor was used to generate the fire emissions and heat flux input for CMAQ simulations (Houyoux et al., 2000).

The first approach calculated emission rates based on actual burning information (location, time, duration, field size, fuel load and burning completeness). Emission factors for $PM_{2.5}$ were based on aerostat measurements and CO was based on aircraft measurements from the field study. The aerostat did not measure CO and the aircraft did not employ a filter-based $PM_{2.5}$ measurement approach so a combination of both platforms is used here. Emission factors for other modeled species (e.g. volatile organic compounds and nitrogen oxides) were based on past studies (Dhammapala et al., 2006; Stockwell et al., 2015).

The second approach for estimating emission rates was based on the method used for crop residue burning emissions in the 2014 NEI (Pouliot et al., 2017). The Pouliot et al., 2017 method estimates emissions with remote sensing data, default field information and literature-based, crop-specific emission factors. The Hazard Mapping System (Ruminski and Hanna, 2008 and Ruminski and Hanna, 2010), which is the satellite product used for providing fire locations developed by the National Oceanic and Atmospheric Administrations (NOAA), detected burns for only one of the sampling days and does not distinguish between the multiple burns at that location. Therefore, fire location and timing were based on actual field study information. Other factors including area burned, fuel load, combustion completeness, and fuel specific (bluegrass and wheat) emission factors were based on default assumptions presented by Pouliot et al., 2017 and used in the 2014 NEI.

2.4. Cropland fire plume rise

Cropland fire emissions have traditionally been injected directly into the surface layer of the model with no treatment for plume rise. However, visual examination of cropland fire plumes and remotely sensed based data suggest cropland fires do have enough heat flux to result in a buoyant plume (Raffuse et al., 2012). Based on past assessments which suggest fires greater than approximately 40 ha experience plume loft (Raffuse et al., 2012), the plume rise approach used for wildland fire in CMAQ is extended for use in cropland fires as a sensitivity test. The modified Briggs approach implemented in CMAQ estimates the plume top and bottom based on buoyancy heat flux (Paugam et al., 2016). The buoyancy heat flux is estimated in SMOKE based on fire size, fuel loading, heat content (always assumed to be 1.6×10^7 BTU/ton), and the duration of the fire (Eq. (1)).

$$\begin{aligned} \mathit{Buoyancy\ Heat\ Flux}\left(\frac{BTU}{s}\right) &= \mathit{Area\ Burned}\ (acre) \\ &\quad \times \text{Fuel Loading}\ (ton/acre) \\ &\quad \times \text{Heat Content}\ (BTU/ton) \\ &\quad \div \mathit{Duration\ of\ fire}\ (s) \end{aligned} \tag{1}$$

2.5. Vertical distribution of cropland fire emissions

Fire emissions are vertically distributed in CMAQ based on estimated combustion phase. The percentage of emissions estimated to be flaming is evenly distributed from the plume bottom to top and the remaining emissions are distributed from the surface layer to plume bottom (Pouliot et al., 2005). Since fire emissions input to CMAQ are not differentiated by combustion phase in this analysis, total emissions are allocated to combustion phase (flaming or smoldering) based on the total area burned in a given hour (Eq. (2)). Residual smoldering phase is not considered separately but as part of the smoldering phase. The percentage of flaming emissions is solely dependent on the acres burned.

$$\text{Flaming}\ (\%) = \ln(\text{acres burned}) * 0.0703 + 0.3 \tag{2}$$

Eq. (2) is based on virtual fire size informed by actual fuel loading and area burned and visual interpretation of smoke vertical distribution using expert opinion (Western Regional Air Partnership, 2004).

The observed MCE for field study burns (>90%) were much larger than the estimated flaming percent based on Eq. (2) (60–66%). This low bias in flaming percentage for these cropland fires means that too much of the emissions will be considered "non-flaming" and distributed closer to the surface as opposed to the buoyant plume. A sensitivity test was done where all emissions were considered to be flaming to be more consistent with combustion components observed during the field study. This means both flaming and residual component emissions will be distributed similarly in the plume, which is consistent with actual conditions since most smoldering emissions will be transported in the same updrafts as the flaming emissions. In this sensitivity, only the vertical distribution of emissions changes, the emissions themselves and the plume rise do not change.

2.6. Description of model simulations

A total of five model simulations were performed for this analysis. The first did not include the cropland burns from the field study and the other four simulations included variations in approach for estimating emissions, plume rise, and vertical distribution of emissions. The contribution from each of the cropland burns was estimated by difference between the simulation where the fire was included and the simulation where the fire was not included. Table 2 shows each of the 5 model simulations along with the corresponding emissions estimation approach, plume rise approach, and vertical allocation of emissions. Table 3 provides more details about emission rates of CO and $PM_{2.5}$ and buoyancy heat flux used for each of the individual burns. A total of 2 CMAQ simulations use field study based emissions and the modified Briggs plume rise approach. They differ in treatment of the vertical allocation of emissions: one uses the default approach for applying Eq. (2) (FIELD_MBRIGGS) and the other modifies Eq. (2) such that all emission are considered flaming (FIELD_FLAMING). One simulation represents the traditional approach for estimating cropland burning emissions in

Table 2
Information about the emissions, plume rise approach, and vertical distribution of emissions used in each CMAQ simulation.

Number	CMAQ simulation name	Emission	Plume rise	Vertical allocation of emissions
1	BASELINE	None	N/A	N/A
2	FIELD_MBRIGGS	Field measurements	Modified BRIGGS using field data for Eq. (1)	CMAQ default Eq. (2) approach
3	FELD_FLAMING	Field measurements	Modified BRIGGS using field data for Eq. (1)	Modified Eq. (2) for 100% flaming
4	POULIOT_MBRIGGS	Pouliot et al., 2017	Modified BRIGGS using default Pouliot et al., 2017 assumptions for Eq. (1)	CMAQ default Eq. (2) approach
5	POULIOT_SURFACE	Pouliot et al., 2017	None	All emissions in surface layer

the National Emission Inventory: emission factors and field size information based on Pouliot et al., 2017 and all emissions are vertically allocated to the surface level (POULIOT_SURFACE). Alternatively, a CMAQ simulation was done using the Pouliot et al., 2017 emission factors and field size assumptions but used the modified Briggs plume rise approach and default approach of using Eq. (2) for vertical emission allocation (POULIOT_MBRIGGS).

3. Results and discussion

3.1. Observations

The total biomass consumed estimates for Burns 1, 2, 3 and 5 at Nez Perce are similar between emissions estimation approaches because underestimates of field size by Pouliot et al., 2017 are compensated by higher assumed fuel loading (Table 1). For Burn 4 at Nez Perce, the total biomass consumed estimated from field measurements is about two times the Pouliot et al., 2017 assumption due to higher fuel loading measured and larger area burned. The opposite is seen at the Walla Walla fields, where the Pouliot et al., 2017 assumed field size is larger than the area burned for field 8, but total biomass consumed is similar to actual values because the fuel loading assumption is lower than observed. Observed fuel consumption was much larger for burn 6 where Pouliot et al., 2017 assumptions for both field size and fuel consumption were much lower than observed. Field size and biomass loading assumptions resulted in large underestimates of fuel consumption for burn 4 at Nez Perce and 6 at Walla Walla. Overall, the average biomass fuel load across all sites and burns is 2.2 tons/acre which is approximately 16% higher than the default assumed for all fields in the Pouliot et al., 2017 approach; average area burned for the fields at Walla Walla and Nez Perce was 160 acres, which is about 30% higher than the default field size; the combustion completeness assumption is 85%, which is similar to the 90% combustion completeness based on post-burn qualitative inspection of the fields. If average field study burn area, fuel load, and combustion completeness were used in place of Pouliot et al., 2017 default values an additional 123 tons (~60% increase) of biomass would be estimated for consumption per burn.

3.2. Emissions

Fig. 4 shows the variability of total biomass loading, emission factors, and total emissions of $PM_{2.5}$ and CO by fuel type for the experiment burns and values based on Pouliot et al., 2017, which was used to support the 2014 National Emission Inventory. The MCEs based on CO and CO_2 emission factors are generally similar between both approaches, which reflect fires dominated by flaming combustion rather than smoldering and both suggest a higher MCE for wheat compared with bluegrass. The $PM_{2.5}$ emission factor for Kentucky bluegrass provided by Pouliot et al., 2017 (11.6 g/kg) falls within the range measured (8.5 to 14.6 g/kg) while the $PM_{2.5}$ emission factor for wheat (4.0 g/kg) is well below the range measured (9.3 to 12.6 g/kg) (Fig. 4). The CO emission factors used in Pouliot et al., 2017 are higher than field measurements for each fuel type.

The total emissions of $PM_{2.5}$ and CO estimated using the Pouliot et al., 2017 method are within the interquartile range of the field data except emissions of $PM_{2.5}$ for wheat, which is slightly lower than measurements. Lower $PM_{2.5}$ emission factors for wheat and lower field size and fuel consumption assumptions made by Pouliot et al., 2017 resulted in lower estimated emission rates compared to using field data. Besides burn 4, the modeled $PM_{2.5}$ emission rates based on Pouliot et al., 2017 for all bluegrass burns match up well with field study based emission rates due to higher emission factors being offset by lower assumptions about area burned and fuel load compared to actual conditions (Table 1). Total CO emissions are generally comparable to field measurements due to underestimated field size and fuel load assumptions offsetting the higher emission factor. However, the CO emission rates estimated by Pouliot et al., 2017 for burns 4 and 6 are much lower than the rates based on field measurements due to the significant underestimation in assumed total biomass consumption.

3.3. Horizontal plume transport

Fig. 5 shows modeled CO with aircraft path and points where the ambient measurements of CO were elevated compared to background overlaid to provide a sense about how the ambient and modeled plumes

Table 3
Buoyancy heat flux, emission rates, and flaming phase percentage used in each model simulation.

Simulation			Burn number						
			1	2	3	4	5	6	8
FIELD_MBRIGGS	Buoyancy heat flux (BTU/s)		7.6×10^6	1.1×10^6	1.1×10^6	1.9×10^6	6.1×10^5	1.5×10^6	9.1×10^5
	Emission rates	CO (mol/s)	76	145	109	281	80	101	50
		$PM_{2.5}$ (g/s)	621	732	563	2000	293	1032	622
	Flaming (%)		66	66	66	66	66	68	60
POULIOT_MBRIGGS	Buoyancy heat flux (BTU/s)		8.6×10^5	8.6×10^5	8.6×10^5	8.6×10^5	4.3×10^5	4.3×10^5	8.6×10^5
	Emission rates	CO (mol/s)	159	159	96	159	79	48	96
		$PM_{2.5}$ (g/s)	564	564	196	564	282	98	196
	Flaming (%)		64						
FIELD_FLAMING	Buoyancy heat flux (BTU/s)		Same as FIELD_MBRIGGS						
	Emission rates		Same as FIELD_MBRIGGS						
	Flaming (%)		100						
POULIOT_SURFACE	Buoyancy heat flux (BTU/s)		0						
	Emission rates		Same as POULIOT_MBRIGGS						
	Flaming (%)		Ignored. All emissions put in the lowest vertical model layer (1)						

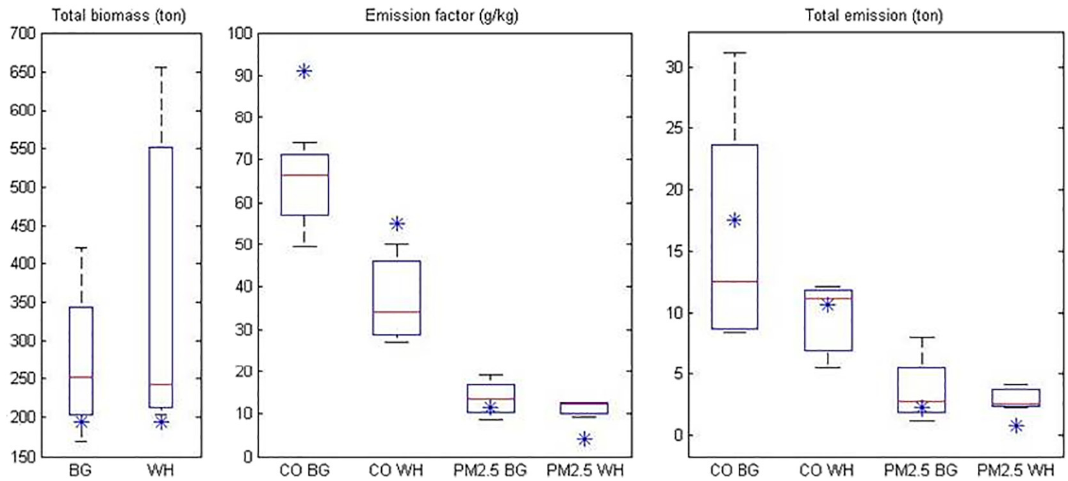

Fig. 4. Total biomass, emission factors, and total emissions of CO and $PM_{2.5}$ based on field study data (red line is the median, box top edge is the 75th percentile, box bottom edge is the 25th percentile, and black lines are the maximum and minimum) and from Pouliot et al., 2017 (stars). (For interpretation of the references to color in this figure legend, the reader is referred to the web version of this article.)

were oriented in horizontal space. Plume impacts shown regionally (Fig. S1) indicate steady modeled winds for each of the burns except for the morning burn on August 19. On August 19, the model does well at capturing the near-fire downwind plume from the morning burn but misses some of the easterly edges of the afternoon burn. The model does very well representing near-fire transport on August 20 at Nez Perce and August 24 at Walla Walla. Meteorological conditions on August 25 at Walla Walla were not well captured by the model, which predicted fairly steady winds from the west even though actual winds were fairly light and disorganized resulting in a meandering plume that generally moved in the opposite direction (Fig. S2). In situations where the model correctly captures local scale meteorology, modeled downwind plume transport compared favorably to aircraft measurements.

The model often estimated lower CO levels compared with aircraft measurements. One contributing factor may be that wind speed predictions were often notably higher than measured at nearby surface stations (Fig. S3). Excessive turbulence may lead to over-dilution of the plume in the near-field. Also, the use of finer grid spacing (<2 km) would likely result in higher model estimates of CO in these plumes (Baker et al., 2014). Model treatment of plume rise and the vertical distribution of emissions may also contribute to this discrepancy and are further examined in subsequent sections.

3.4. Plume rise

Modeled CO is shown by model layer for each of the field burns at Nez Perce in Fig. 6 and Walla Walla in Fig. 7 with the surface mixing layer height estimated by the ceilometer and plume top observed by the lidar. The daily boundary layer evolution has a major influence on the concentration of airborne substances near the surface, because the extent of vertical mixing is usually limited by the boundary layer top. The surface mixing layer height estimated by WRF is well characterized for these locations, indicating reasonable boundary layer constraints for the study period (Figs. 6 and 7). Short-term extreme variability in surface mixing layer height estimated by the ceilometer are likely related to brief smoke impacts and not indicative of vertical mixing in the area. Lidar observations from the field experiment often indicate a higher plume top than boundary layer top. For example, on August 20 the lidar detected plume top of about 2000 m is higher than the ceilometer detected boundary layer top at approximately 1600 m at Nez Perce

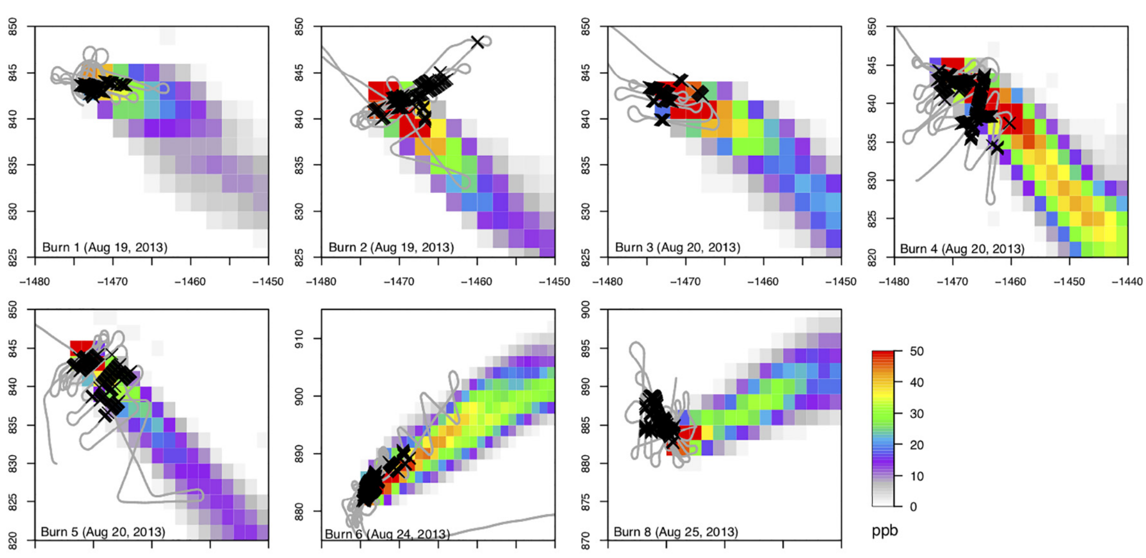

Fig. 5. Modeled CO levels are shown for each of the burns at Nez Perce and Walla Walla. The aircraft flight path is shown with the gray trace and instances where measured CO was well above background levels are shown with black crosses to illustrate the densest area of the ambient smoke plume.

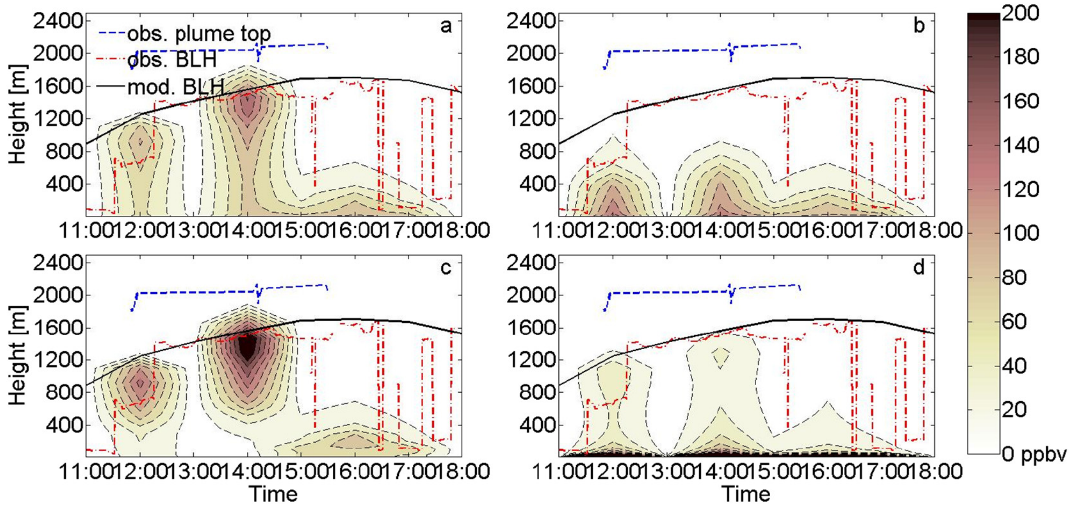

Fig. 6. Color-filled contours of simulated CO (ppb) due to fire emissions at Nez Perce on August 20 (a – FIELD_MBRIGGS, b – POULIOT_MBRIGGS, c – FIELD_FLAMING, d – POULIOT_SURFACE) superimposed with ceilometer detected boundary layer height, model input boundary layer height, and lidar estimated plume top. The plume edge is the 20 ppbv contour line. (For interpretation of the references to color in this figure legend, the reader is referred to the web version of this article.)

(Fig. 6 and S4). Although the lidar and ceilometer data shows notable variability at Walla Walla, the detected plume top is still consistently higher than the boundary layer top (Fig. 7). In addition, aircraft measurements also captured high CO levels above the ceilometer estimated boundary layer top (Fig. S4).

The model simulations using the lower emissions and buoyancy heat flux (POULIOT_MBRIGGS and POULIOT_SURFACE) have plume tops well below lidar observations (Fig. 6). The use of the wildland fire plume rise approach in CMAQ (POULIOT_MBRIGGS) provides a more realistic smoke plume compared to injecting emissions at the surface. Placement of all smoke emissions at the surface (POULIOT_SURFACE) results in an unrealistic plume bifurcation where concentrations are highest at the surface and at the top of the surface mixing layer with less in between. This is due to the Asymmetric Convection Model (ACM) vertical diffusion scheme in CMAQ (Pleim, 2007), which limits pollutant transport only between adjacent layers except for the surface layer. Unlike non-surface layers, emissions in the surface layer can be quickly transported to all other layers within the boundary layer. This approach is designed to move mass from the surface efficiently throughout the boundary layer while moving pollutants between non-surface layers comparatively slower. When high concentrations are at the surface, as in the case of POULIOT_SURFACE, this mixing scheme will result in both high surface and comparatively higher concentrations at the top of the boundary layer than what may be estimated using a plume rise approach (e.g., POULIOT_MBRIGGS).

In the simulations with higher buoyancy heat flux (FIELD_MBRIGGS and FIELD_FLAMING), fire emitted CO gets transported above the model boundary layer top, exhibiting better agreement with the observed plume top height than the other two simulations (Fig. 6). The reason for the improvement in plume rise is likely related to the more realistic heat flux estimates based on actual field information. The input buoyancy heat flux for burns on August 20 estimated with actual field conditions is 30% to 120% higher than the fluxes estimated based on assumptions, which results in a plume height increase of 300 m to 800 m or by 30% to 80% (Table 3 and Fig. 6). For the burn at Walla Walla on August 24, the input heat flux based on actual field conditions

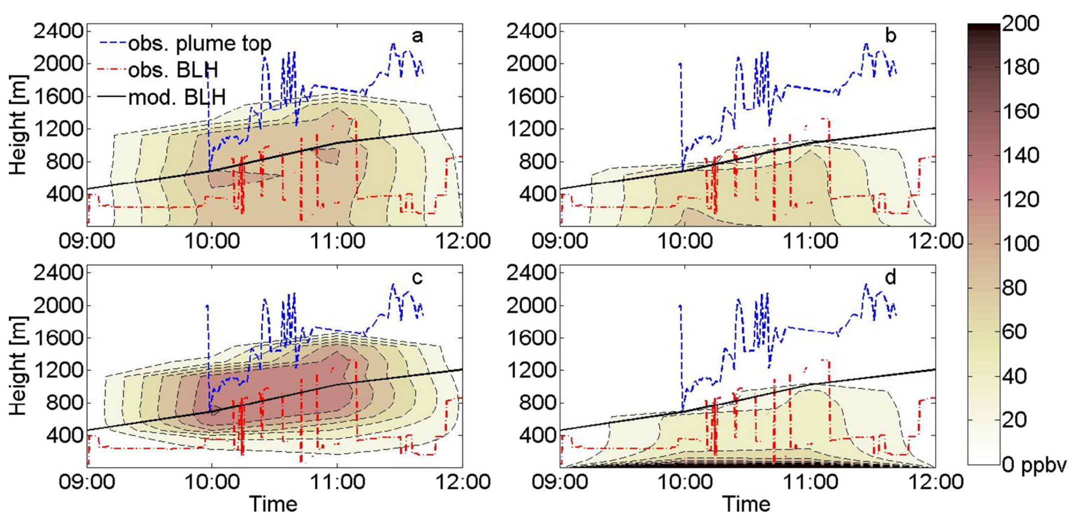

Fig. 7. Color-filled contours of simulated CO (ppb) due to fire emissions at Walla Walla on August 24 (a – FIELD_MBRIGGS, b – POULIOT_MBRIGGS, c – FIELD_FLAMING, d – POULIOT_SURFACE) superimposed with ceilometer detected boundary layer height, model input boundary layer height, and lidar estimated plume top. The plume edge is the 20 ppbv contour line. (For interpretation of the references to color in this figure legend, the reader is referred to the web version of this article.)

is more than three times the flux based assumptions, which results a plume top increase by 600 m or by 60% and better agreement with lidar estimated plume top (Fig. 7).

Treating cropland fire emissions with a buoyant plume rise as opposed to placement of all emissions at the surface improved comparison with lidar predicted plume tops. Further, using actual field conditions including area burned and fuel consumption also resulted in better comparison with plume top observations at these field burns. It should also be noted that an improved temporal resolution of model heat flux input could potentially improve the model estimated plume rise. For instance, some of the burns at Nez Perce lasted approximately an hour, but the most intense flaming and resulting plume buoyancy was during a shorter timespan within that hour. Consequently, the buoyancy heat flux would be slightly higher (Eq. (1)) at Nez Perce creating higher plumes. The fields at Walla Walla were ignited section by section and the burns went for a longer time. Since the Walla Walla fires were more evenly distributed temporally across a longer period, plume rise was lower than at Nez Perce and resulted better agreement with the model prediction.

3.5. Vertical distribution of emissions

Surface levels of pollutants are impacted by plume direction, plume height as that defines the vertical column space that emitted material are mixed, and also the vertical allocation of emissions in the plume column. Fig. 8 shows ambient CO measured by aircraft and modeled average CO due to field burning by vertical layer over all hours of burning for four different field study days. As indicated by the average vertical profile of CO in Fig. 8, surface levels are higher using assumed field information to inform heat flux calculations (POULIOT_MBRIGGS) which resulted in lower plume heights compared to modeled plumes informed with actual field information (FIELD_MBRIGGS). The differences in plume height are notable even though the FIELD_MBRIGGS simulation had higher CO emissions (Table 3). The CO emission rates used in FIELD_MBRIGGS approach is two times higher than POULIOT_MBRIGGS, however, the simulated surface CO concentration is only about 10% higher in FIELD_MBRIGGS due to the higher (60%) estimated plume height.

The vertical allocation of emissions within the plume top and bottom directly impacts the predicted column distribution of smoke from these fires. The FIELD_FLAMING simulation provides an alternative vertical distribution of emissions compared to FIELD_MBRIGGS by modifying Eq. (2) so that all emissions regardless of component (e.g., flaming to smoldering) would be distributed within the buoyant plume. Further, it is likely that most of the smoldering phase emissions concurrent with flaming during these fires would be lofted in the same convective plume updraft and have similar near-fire downwind transport. As shown by Figs. 6 and 7, changing the vertical distribution of emissions (FIELD_FLAMING) does not change the plume height, but decreases the amount of emitted material at the surface and increases the amount emitted material at higher layers when compared to the standard CMAQ approach of allocating a fraction of emissions between the surface layer and bottom of the buoyant plume (FIELD_MBRIGGS and POULIOT_MBRIGGS). The simulated surface CO concentration at Nez Perce decreased approximately 40% to 60% due to emissions being injected at higher vertical levels in the model while it decreases about 30% to 90% for burns at Walla Walla (green and red curves in Fig. 8). Alternatively, the CO levels at higher altitudes in the boundary layer estimated by the FIELD_FLAMING simulation agree the best with aircraft measurements.

The aircraft profile does not provide information about surface CO levels. Surface $PM_{2.5}$ measurements (EBAMS) were deployed very close each of the burns (Figs. 2 and 3) but not available aloft. Given the proximity between the EBAMs and the field burns, this data is more relevant for emission factors and less reflective of the 2 km grid scale used in this modeling system.

4. Conclusions

This field study provided a unique opportunity to constrain multiple aspects of the fuels and emissions that impact photochemical grid model representation of near-fire plume transport and prediction of primarily emitted pollutants like CO and $PM_{2.5}$. The Pouliot et al., 2017 default emission factors for Kentucky bluegrass CO may need to be revised to a lower value and wheat $PM_{2.5}$ to a higher value for this region for future model applications. Further, improvements to regional specific assumptions for field size, fuel load, and fuel consumption may be needed to better represent plume rise from cropland fires in this area. Measurements of the surface mixing layer height during the field studies was matched well by the modeling system indicating that diurnal variability

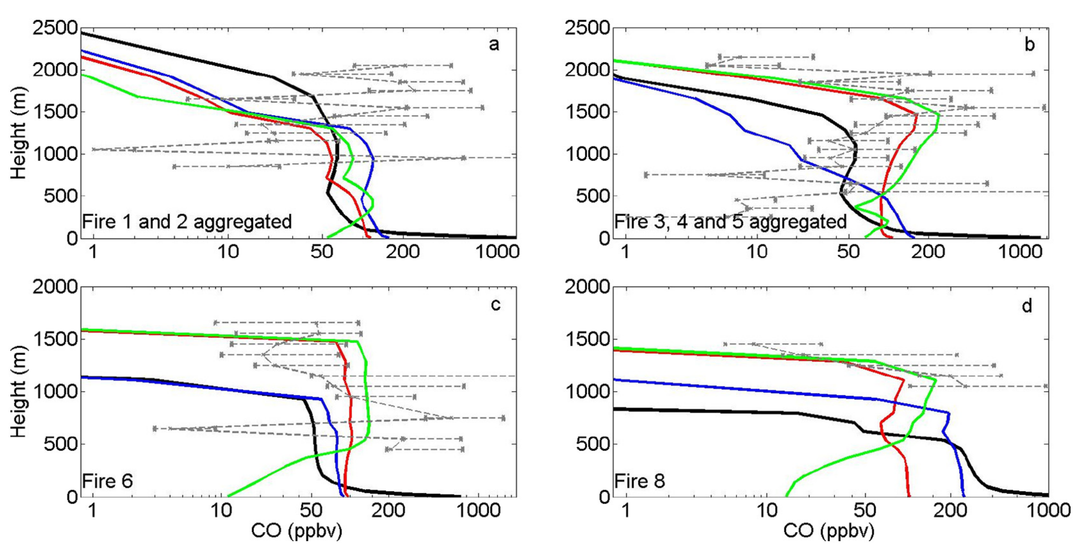

Fig. 8. Average vertical profile of simulated CO from fire (solid lines, black—POULIOT_SURFACE, red—FIELD_MBRIGGS, blue—POULIOT_MBRIGGS, green—FIELD_FLAMING) and the distribution of CO from aircraft measurements (dashed line) during the time period of burning for each day at Nez Perce on a) August 19 and b) August 20 and at Walla Walla on c) August 24 and d) August 25. The distribution of aircraft CO measurements is shown by vertical layer and extends from the 25th to 75th quantile. (For interpretation of the references to color in this figure legend, the reader is referred to the web version of this article.)

in the vertical mixing layer height is well characterized and not contributing to differences between model and ambient chemical measurements. Horizontal transport of fire plumes was fairly well characterized by the modeling system, but micro-scale meteorological features were not always well captured which sometimes hindered representation of local scale transport.

The results of this study suggest the traditional approach of injecting all cropland burning emissions into the surface layer of the modeling system does not realistically represent vertical plume structure for these sized fires (or larger). The modified Briggs based plume rise approach does well representing plume height compared to lidar observations, especially when actual acres burned are used to estimate heat flux and the timing of the fire is well represented. The buoyancy heat flux estimated for these fires could only be indirectly evaluated here and future work is needed to more directly evaluate and improve heat flux estimates for fires. Vertical allocation of emissions needs further study and was difficult to constrain with the data available from this field study. This is especially needed for allocation of the residual smoldering, since those emissions would not be expected to be coincident with the large buoyancy heat flux related to initial stages of burning.

Acknowledgment

We would also like to thank the field study participants for providing data: B. Gullett, A. Holder, J. Aurell, W. Mitchell, V. Kovalev, W. Hao, and J. Vaughan.; and contribution from others including J. Wilkins. This research was performed while Luxi Zhou held a National Research Council Research Associateship Award at the United States Environmental Protection Agency.

Disclaimer

Although this work was reviewed by EPA and approved for publication, it may not necessarily reflect official agency policy.

Appendix A. Supplementary data

Supplementary data to this article can be found online at https://doi.org/10.1016/j.scitotenv.2018.01.237.

References

Aurell, J., Gullett, B.K., 2013. Emission factors from aerial and ground measurements of field and laboratory forest burns in the southeastern US: $PM_{2.5}$, black and brown carbon, VOC, and PCDD/PCDF. Environ. Sci. Technol. 47:8443–8452. https://doi.org/10.1021/ES402101K.

Aurell, J., Gullett, B.K., Tabor, D., Williams, R.K., Mitchell, W., Kemme, M.R., 2015. Aerostat-based sampling of emissions from open burning and open detonation of military ordnance. J. Hazard. Mater. 284, 108–120.

Baker, K., Hawkins, A., Kelly, J.T., 2014. Photochemical grid model performance with varying horizontal grid resolution and sub-grid plume treatment for the Martins Creek near-field SO2 study. Atmos. Environ. 99, 148–158.

Baker, K., Woody, M., Tonnesen, G., Hutzell, W., Pye, H., Beaver, M., Pouliot, G., Pierce, T., 2016. Contribution of regional-scale fire events to ozone and $PM_{2.5}$ air quality estimated by photochemical modeling approaches. Atmos. Environ. 140, 539–554.

Bash, J.O., Baker, K.R., Beaver, M.R., 2016. Evaluation of improved land use and canopy representation in BEIS v3. 61 with biogenic VOC measurements in California. Geosci. Model Dev. 9:2191–2207. https://doi.org/10.5194/gmd-9-2191-2016.

Byun, D.W., Schere, K.L., 2006. Review of the governing equations, computational algorithms, and other components of the Models-3 Community Multiscale Air Quality (CMAQ) Modeling System. Appl. Mech. Rev. 59, 51–77.

Carlton, A.G., Bhave, P.V., Napelenok, S.L., Edney, E.O., Sarwar, G., Pinder, R.W., Pouliot, G.A., Houyoux, M., 2010. Treatment of secondary organic aerosol in CMAQv4.7. Environ. Sci. Technol. 44, 8553–8560.

Dhammapala, R., Claiborn, C., Corkill, J., Gullett, B.K., 2006. Particulate emissions from wheat and Kentucky bluegrass stubble burning in eastern Washington and northern Idaho. Atmos. Environ. 40 (6), 1007–1015.

Fann, N., Fulcher, C.M., Baker, K., 2013. The recent and future health burden of air pollution apportioned across US sectors. Environ. Sci. Technol. 47, 3580–3589.

Foley, K.M., Roselle, S.J., Appel, K.W., Bhave, P.V., Pleim, J.E., Otte, T.L., Mathur, R., Sarwar, G., Young, J.O., Gilliam, R.C., Nolte, C.G., Kelly, J.T., Gilliland, A.B., Bash, J.O., 2010. Incremental testing of the Community Multiscale Air Quality (CMAQ) modeling system version 4.7. Geosci. Model Dev. 3:205–226. https://doi.org/10.5194/gmd-3-205-2010.

Forster, P., et al., 2007. Changes in atmospheric constituents and in radiative forcing. In: Solomon, S., Qin, D., Manning, M., Chen, Z., Marquis, M., Averyt, K.B., Tignor, M., Miller, H.L. (Eds.), Climate Change 2007: The Physical Science Basis. Contribution of Working Group I to the Fourth Assessment Report of the Intergovernmental Panel on Climate Change. Cambridge University Press, Cambridge, U. K. and New York, NY, USA.

Fountoukis, C., Nenes II, A. Isorropia, 2007. A computationally efficient thermodynamic equilibrium model for K^+-Ca^{2+}-Mg^{2+}-Nh(4)(+)-Na+-$SO4_2$–NO_3–Cl–H_2O aerosols. Atmos. Chem. Phys. 2007 (7), 4639–4659.

Garcia-Menendez, F., Hu, Y., Odman, M.T., 2013. Simulating smoke transport from wildland fires with a regional-scale air quality model: sensitivity to uncertain wind fields. J. Geophys. Res. Atmos. 118:6493–6504. https://doi.org/10.1002/jgrd.50524.

Garcia-Menendez, F., Hu, Y., Odman, M.T., 2014. Simulating smoke transport from wildland fires with a regional-scale air quality model: sensitivity to spatiotemporal allocation of fire emissions. Sci. Total Environ. 493, 544–553.

Henderson, B., Akhtar, F., Pye, H., Napelenok, S., Hutzell, W., 2014. A database and tool for boundary conditions for regional air quality modeling: description and evaluation. Geosci. Model Dev. 7, 339–360.

Holder, A., Gullett, B.K., Urbanski, S.P., Elleman, R., O'Neill, S., Tabor, D., Mitchell, W., Baker, K.R., 2017. Emissions from prescribed burning of agricultural fields in the Pacific northwest. Atmos. Environ. 166:22–33. https://doi.org/10.1016/j.atmosenv.2017.06.043.

Houyoux, M.R., Vukovich, J.M., Coats Jr., C.J., Wheeler, N.J.M., Kasibhatla, P.S., 2000. Emission inventory development and processing for the Seasonal Model for Regional Air Quality (SMRAQ) project. J. Geophys. Res. 105, 9079–9090.

Jain, R., Vaughan, J., Heitkamp, K., Ramos, C., Claiborn, C., Schreuder, M., Schaaf, M., Lamb, B., 2007. Development of the ClearSky smoke dispersion forecast system for agricultural field burning in the Pacific Northwest. Atmos. Environ. 41 (7645-6761). https://doi.org/10.1016/j.atmosenv.2007.04.058.

Kovalev, V., Petkov, A., Wold, C., Urbanski, S., Hao, W.M., 2015. Determination of the smoke-plume heights and their dynamics with ground-based scanning lidar. Appl. Opt. 54 (8):2011–2017. https://doi.org/10.1364/AO.54.002011.

Larkin, N.K., O'Neill, S.M., Solomon, R., Raffuse, S., Strand, T., Sullivan, D., Krull, C., Rorig, M., Peterson, J., Ferguson, S.A., 2009. The BlueSky smoke modeling framework. Int. J. Wildland Fire 18, 906–920.

Larkin, N.K., Strand, T.M., Drury, S.A., Raffuse, S.M., Solomon, R.C., O'Neill, S.M., Wheeler, N., Huang, S.M., Rorig, M., Hafner, H.R., 2012. Final Report to the JFSP for Project #08-1-7-10: Phase 1 of the Smoke and Emissions Model Intercomparison Project. http://firescience.gov.

Liu, J.C., Pereira, G., Uhl, S.A., Bravo, M.A., Bell, M.L., 2015. A systematic review of the physical health impacts from non-occupational exposure to wildfire smoke. Environ. Res. 136, 120–132.

Liu, J.C., Wilson, A., Mickley, L.J., Dominici, F., Ebisu, K., Wang, Y., Sulprizio, M.P., Peng, R.D., Yue, X., Anderson, G.B., 2016. Wildfire-specific fine particulate matter and risk of hospital admissions in urban and rural counties. Epidemiology 28 (1):77–85. https://doi.org/10.1097/EDE.0000000000000556.

McCarty, J.L., 2011. Remote sensing-based estimates of annual and seasonal emissions from crop residue burning in the contiguous United States. J. Air Waste Manage. Assoc. 61 (1):22–34. https://doi.org/10.3155/1047-3289.61.1.22.

McCarty, J.L., Korontzi, S., Justice, C.O., Loboda, T., 2009. The spatial and temporal distribution of crop residue burning in the contiguous United States. Sci. Total Environ. 407 (2009), 5701–5712.

NCAR, 2008. A Description of the Advanced Research WRF Version 3; NCAR Technical Note NCAR/TN-475+STR. Boulder, CO, National Center for Atmospheric Research: p. 2008. http://www2.mmm.ucar.edu/wrf/users/docs/arw_v3.pdf.

Paugam, R., Wooster, M., Freitas, S., Val Martin, M., 2016. A review of approaches to estimate wildfire plume injection height within large-scale atmospheric chemical transport models. Atmos. Chem. Phys. 16:907–925. https://doi.org/10.5194/acp-16-907-2016.

Pleim, J.E., 2007. A combined local and nonlocal closure model for the atmospheric boundary layer. Part I: model description and testing. J. Appl. Meteorol. Climatol. 46, 1383–1395.

Pouliot, G., Pierce, T., Benjey, W., O'Neill, S.M., Ferguson, S.A., 2005. Wildfire emission modeling: integrating BlueSky and SMOKE. Presentation at the 14th International Emission Inventory Conference, Transforming Emission Inventories Meeting Future Challenges Today, 4/11–4/14/05 Las Vegas, NV.

Pouliot, G., Rao, V., McCarty, J.L., Soja, A., 2017. Development of the crop residue and rangeland burning in the 2014 National Emissions Inventory using information from multiple sources. J. Air Waste Manage. Assoc. 67 (5):613–622. https://doi.org/10.1080/10962247.2016.1268982.

Raffuse, S.M., Craig, K.J., Larkin, N.K., Strand, T.T., Sullivan, D.C., Wheeler, N.J., Solomon, R., 2012. An evaluation of modeled plume injection height with satellite-derived observed plume height. Atmosphere 3, 103–123.

Rappold, A.G., Stone, S.L., Cascio, W.E., Neas, L.M., Kilaru, V.J., Sue Carraway, M., Szykman, J.J., Ising, A., Cleve, W.E., Meredith, J.T., 2011. Peat bog wildfire smoke exposure in rural North Carolina is associated with cardiopulmonary emergency department visits assessed through syndromic surveillance. Environ. Health Perspect. 119 (10): 1415–1420. https://doi.org/10.1289/ehp.1003206.

Reid, C.E., Brauer, M., Johnston, F., Jerrett, M., Balmes, J.R., Elliott, C.T., 2016. Critical review of health impacts of wildfire smoke exposure. Environ. Health Perspect. 124 (9): 1334–1343. https://doi.org/10.1289/ehp.1409277.

Ruminski, M., Hanna, J., 2010. A validation of automated and quality controlled satellite based fire detection. AGU Fall Meeting 2010, San Francisco, California.

Sarwar, G., Appel, K.W., Carlton, A.G., Mathur, R., Schere, K., Zhang, R., Majeed, M.A., 2011. Impact of a new condensed toluene mechanism on air quality model predictions in the US. Geosci. Model Dev. 4, 183–193.

Sarwar, G., Fahey, K., Kwok, R., Gilliam, R.C., Roselle, S.J., Mathur, R., Xue, J., Yu, J., Carter, W.P.L., 2013. Potential impacts of two SO2 oxidation pathways on regional sulfate concentrations: aqueous-phase oxidation by NO2 and gas-phase oxidation by stabilized Criegee intermediates. Atmos. Environ. 68, 186–197.
Seaman, N.L., 2000. Meteorological modeling for air-quality assessments. Atmos. Environ. 34 (12–14):2231–2259. https://doi.org/10.1016/S1352-2310(99)00466-5.
Stockwell, C.E., Veres, P.R., Williams, J., Yokelson, R.J., 2015. Characterization of biomass burning emissions from cooking fires, peat, crop residue, and other fuels with high-resolution proton-transfer-reaction time-of-flight mass spectrometry. Atmos. Chem. Phys. 15:845–865. https://doi.org/10.5194/acp-15-845-2015.
U.S. EPA, 2003. Cereal-grain residue open-field burning emissions study. Washington Department of Ecology, Washington Association of Wheat Growers, U.S. Environmental Protection Agency, Region 10. Air Sciences Inc., Portland, OR and Golden CO http://www.ecy.wa.gov/programs/air/pdfs/FinalWheat_081303.pdf.
U.S. EPA, 2016. U.S. Environmental Protection Agency, Technical Support Document (TSD) Preparation of Emissions Inventories for the Version 6.3, 2011 Emissions Modeling Platform. https://www.epa.gov/air-emissions-modeling/2011-version-63-technical-support-document.
Urbanski, S.P., Hao, W.M., Nordgren, B., 2011. The wildland fire emission inventory: western United States emission estimates and an evaluation of uncertainty. Atmos. Chem. Phys. 11:12973–13000. https://doi.org/10.5194/acp-11-12973-2011.
USDA Forest Service, 1998. FMI/WESTAR Emissions Inventory and Spatial Data for the Western United States. USDA Forest Service, Rocky Mountain Research Station, Fire Sciences Laboratory, Missoula, MT.
Washington State University, 2004. Quantifying Post-harvest Emissions from Bluegrass Seed Production Field Burning. Department of Crop and Soil Sciences, Washington State University, Washington, DC:p. 2004. www.ecy.wa.gov/programs/air/aginfo/research_pdf_files/FinalKBGEmissionStudyReport_4504.pdf.
Western Regional Air Partnership, 2004. 2002 Fire Emission Inventory for the WRAP Region Phase I – Essential Documentation. 2004. Western Governors Association/Western Regional Air Partnership. http://www.wrapair.org/forums/fejf/documents/emissions/WRAP_2002%20EI%20Report_20050107.pdf.
Wiedinmyer, C., Hurteau, M., 2010. Prescribed fire as a means of reducing forest carbon emissions in the western United States. Environ. Sci. Technol. 44, 1926–1932.
Yu, P., Toon, O.B., Bardeen, C.G., Bucholtz, A., Rosenlof, K.H., Saide, P.E., Da Silva, A., Ziemba, L.D., Thornhill, K.L., Jimenez, J.-L., Campuzano-Jost, P., Schwarz, J., Perring, A.E., Froyd, K.D., Wagner, N.L., Mills, M.J., Reid, J.S., 2016. Surface dimming by the 2013 Rim Fire simulated by a sectional aerosol model. J. Geophys. Res. Atmos. 121 (12):7079–7087. https://doi.org/10.1002/2015JD024702.